cells, the number (cells/mm^2/mouse) of single stranded DNA (ss-DNA)$^+$ cells in one field in the ischemic core from each mouse in the saline- or hES-ECs+MCs-injected group was quantified at ×20 magnification on day 14 after MCAo.

Neurological Functional test

We used the rota-rod exercise machine for the assessment of the recovery of impaired motor function after MCAo. This accelerating rota-rod test was carried out as described in A.J. Hunter et al. [15] with slight modification. Each mouse was trained up to be able to keep running on the rotating rod over 60 seconds at 9 round per minutes (rpm) (2th speed). After the training was completed, we placed each mouse on the rod and changed the speed of rotation every 10 seconds from 6 rpm (1st speed) to 30 rpm (5th speed) over the course of 50 seconds and checked the time until the mouse fell off. The exercise time (seconds) on the rota-rod for each mouse was recorded just before the experiments (= day 0) and on day 7 and 28 after MCAo.

Analysis of mRNA expression of angiogenic factors

Cultured human aortic smooth muscle cells (hAoSMC) (Cambrex, East Rutherford, NJ) were used for control. Total cellular RNA was isolated from hES-MCs and human aortic smooth muscle cells (hAoSMC) (Cambrex, East Rutherford, NJ) with RNAeasy Mini Kit (QIAGEN K.K., Tokyo, Japan). The mRNA expression was analyzed with One Step RNA PCR Kit (Takara, Out, Japan). The primers used were as follows: human vascular endothelial growth factor (VEGF, Genbank accession No.X62568), 5'-AGGGCAGAATCATCACGAAG-3' (forward) and 5'-CGCTCCGTCGAACTCAATTT-3' (reverse); human basic fibroblast growth factor (bFGF, Genbank accession No.M27968), AGAGCGACCCTCACATCAAG (forward) and TCGTTTCAGTGCCACATACC (reverse); human hepatic growth factor (HGF, Genbank accession No.X16323), 5'-AGTCTGTGACATTCCTCAGTG-3' (forward) and 5'-TGAGAATCCCAACGCTGACA-3' (reverse); human platelet-derived growth factor (PDGF-B, Genbank accession No.X02811), 5'-GCACACGCATGACAA-GACGGC-3' (forward) and 5'-AGGCAGGCTATGCTGA-GAGGTCC-3' (reverse); and GAPDH (Genbank accession No.M33197), 5'-TGCACCACCAACTGCTTAGC-3' (forward) and 5'-GGCATGGACTGTGGTCATGA-3' (reverse). Polymerase chain reactions (PCR) were performed as described in the manufacturer's protocols.

Measurement of angiogenic factors in hES-MCs-conditioned media

After 1 × 10^6 cells of hES-MC or hAoSMC were plated on 10 cm type IV collagen-coated dishes and incubated with 5 ml media (αMEM with 0.5% bovine serum) for 72 hours, the concentration of human VEGF, bFGF and HGF were measured by SRL, Inc. (Tokyo, Japan).

Statistical analysis

All data were expressed as mean ± standard error (S.E.). Comparison of means between two groups was performed with Student's t test. When more than two groups were compared, ANOVA was used to evaluate significant differences among groups, and if there were confirmed, they were further examined by means of multiple comparisons. Probability was considered to be statistically significant at $P < 0.05$.

Results

Preparation and characterization of transplanted cells derived from human ES cells

We induced differentiation of human ES cells in an in vitro two-dimensional culture on OP9 stromal cell line and examined the expression of VEGF-R2, VE-cadherin and TRA-1 during the differentiation. While the population of VE-cadherin$^+$VEGF-R2$^+$TRA-1$^-$ cells was not detected (< 0.5%) before day 8 of differentiation, it emerged and accounted for about 1–2% on day10 of differentiation (Figure 2A). As we previously reported, these VE-cadherin$^+$VEGF-R2$^+$TRA-1$^-$ cells on day 10 of differentiation were also positive for CD34, CD31 and eNOS [10]. Therefore, we used the term 'eEC' for these ECs in the early differentiation stage. We sorted and expanded these eECs in vitro. These eECs were cultured in the presence of VEGF and 10% FCS and expanded by about 85-fold after 5 passages. The expanded cells at 5th passage were constituted with two cell fractions. One of these cells was VE-cadherin$^+$ cells (35–50%), which were positive for other endothelial markers, including CD31 (Figure 2B–E) and CD34 [10], indicating that cell differentiation stage had been retained. The other was VE-cadherin$^-$ cells (50–65%), which were positive for αSMA and considered to differentiate into MCs (Figure 2D–E). We sorted the fraction of VE-cadherin$^-$VEGF-R2$^+$TRA-1$^-$ cells, which appeared on day 8 of differentiation and were positive for platelet derived growth factor receptor type β (PDGFR-β) [10], and expanded these cells for induction to MC in the presence of PDGF-BB and 1% FCS. At passage 5, all of the expanded cells effectively differentiated into αSMA-positive MCs (Figure 2F–G).

Assessment of cerebral blood flow recovery in the infarct area after the transplantation

As shown in Figure 3B, the cerebral blood flow in the ipsilateral side decreased by approximately 80% compared to that in the contralateral side during MCAo and the area with the suppressed blood flow was corresponded to the area under MCA. In the 5 groups, the CBF ratio on day 4 decreased by about 20% compared to that of the contralateral side due to ligation of the left CCA after the trans-

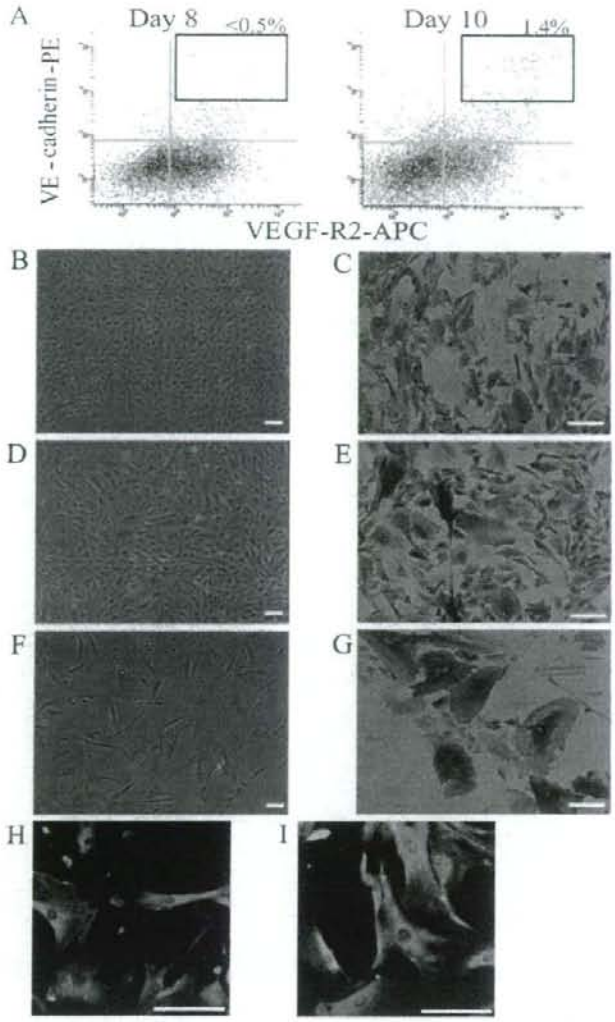

Figure 2

Characterization of the transplanted vascular cells derived from human ES cells (HES-3). A, Flow cytometric analysis of VE-cadherin and VEGF-R2 expression on human ES cells during differentiation on an OP9 feeder layer. VE-cadherin$^+$VEGF-R2$^+$TRA-1$^-$ cells are indicated by the boxed areas. B, Morphology of the VE-cadherin$^+$ cells (= hES-ECs) resorted from expanded VE-cadherin$^+$VEGF-R2$^+$TRA-1$^-$ cells at 5th passage. C, Immunostaining for human PECAM-1 (brown) of hES-ECs. D, Morphology of the expanded VE-cadherin$^+$VEGF-R2$^+$TRA-1$^-$ cells at 5th passage (= hES-ECs+MCs). E, Double immunostaining for human PECAM-1 (brown) and αSMA (purple) on hES-ECs+MCs. F, Morphology of the cells (= hES-MCs) expanded from VE-cadherin$^-$VEGF-R2$^+$TRA-1$^-$ cells on day 10 of differentiation with PDGF-BB and 1% FCS up to 5th passage. G, Immunostaining for αSMA (brown) of hES-MCs. H-I, Immunostaining for αSMA (green) and calponin (red) of hAoSMCs (H) and hES-MCs (I). Scale bar: 50 μm.

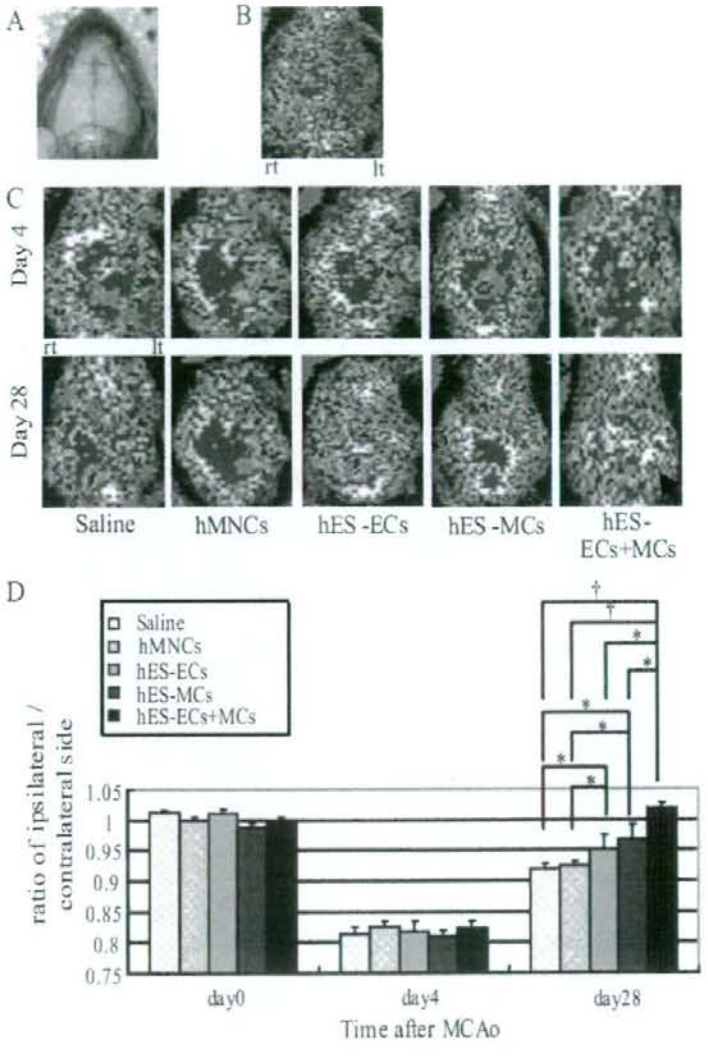

Figure 3

Effects of the transplanted vascular cells on the CBF in the ipsilateral side. A-C: LDPI analysis of the CBF by LDPI evaluated in mice with the scalp removed (A). Flowmetric analysis of the CBF in the ipsilateral side (= left side: lt) during MCA-occlusion (B). The CBF in the ipsilateral and contralateral side in the five groups on day 4 and 28 after MCAo (C). An arrow indicates the lesion in the hES-EC+MC-injected group where the CBF clearly increased up to or rather than the corresponding area in the contralateral side. Red or white indicates higher flow than blue or green. D, Quantitative analysis of the CBF ratio of the ipsilateral/contralateral side just before the experiments (= day 0) and on day 4 and 28 after MCAo. * $P < 0.05$, † $P < 0.01$.

plantation. Then, we assessed the recovery of the CBF in the ipsilateral side from this time point. Apparent difference in the CBF in the ipsilateral side was not observed among the 5 groups on day 4 after MCAo. However, the blood flow of the ipsilateral side in the hES-EC+MC-injected group, especially pointed out by the arrow, clearly increased up to or rather than the corresponding area in the contralateral side on day 28 after MCAo, compared to other 4 groups (Figure 3C). On day 28, the CBF ratio of the saline- and hMNC-injected group were similar (Figure 3D), while that of hES-EC-injected group increased significantly compared to that of these two groups (saline: 0.919 ± 0.010, n = 12. hMNCs: 0.925 ± 0.008, n = 15. hES-ECs: 0.952 ± 0.025, n = 7. $P < 0.05$). The CBF ratio of the hES-MC-injected group (0.968 ± 0.023, n = 7. $P < 0.05$) increased significantly compared to that of the saline- or hMNCs-injected groups on day 28, while that of the hES-EC+MC-injected group (1.018 ± 0.009: n = 13) increased significantly compared to not only that of the saline- or hMNCs-injected groups ($P < 0.001$), but also that of the hES-EC- or hES-MC-injected group ($P < 0.01$).

Localization of transplanted vascular cells derived from human ES cells and the vascular density in the infarct area after the transplantation

In the saline- and hMNCs-injected groups, the vascular density of host capillary quantified by mouse PECAM-1 immunoreactivity in the ischemic striatum (Figure 4B, C) was higher than that in the non-ischemic striatum (Figure 4A). In hMNCs-injected group, few human PECAM-1 positive cells were observed in the ischemic striatum (Figure 4C) and these cells were not found in the non-ischemic striatum. In the hES-EC-injected group, many DiI positive hES-ECs were observed in the infarct area (Figure 4D) and incorporated into the host capillaries (Figure 4E). In the hES-MC-injected group, both αSMA and human HLA positive cells (23.1 ± 2.0 counts/field: n = 7) were detected in the infarct area (Figure 4F) and localized in the conjunction with mouse endothelial tubes (Figure 4G). Compatible with these results, in the hES-EC+MC-injected group, many human PECAM-1 positive cells were detected in the host capillaries (Figure 4H) while transplanted MCs (21.7 ± 1.8 counts/field: n = 6) surrounded the capillaries in the infarct area, similarly to those in the hES-MCs-injected group (Figure 4I).

In the ischemic striatum, the density (%area) of human PECAM-1 positive cells was 0.05 ± 0.01% in the hMNC-injected group (n = 11), 0.66 ± 0.11% in the hES-EC-injected group (n = 7, $P < 0.0001$ vs hMNCs) and 0.85 ± 0.12% in the hES-EC+MC-injected group (n = 11, $P < 0.0001$ vs hMNCs) (Figure 5A). As shown in Figure 5B, there was no significant difference in the densities of mouse PECAM-1 positive cells among the saline- (10.3 ± 0.4%: n = 11), hMNC- (10.9 ± 0.3%: n = 11) and hES-EC- (11.4 ± 0.4%: n = 7) injected groups, although the densities were significantly higher than that in the non-ischemic striatum (5.6 ± 0.2%: n = 5). In hES-MC- (13.2 ± 0.5%: n = 7, $P < 0.01$ vs control, $P < 0.05$ vs hES-ECs) or hES-EC+MC- (13.8 ± 0.4%: n = 11, $P < 0.01$ vs control and hES-ECs) injected group, a significant increase in the density of mouse PECAM-1 positive cells was observed. The total vascular density estimated by summing up human and mouse PECAM-1 positive area (12.2 ± 0.6%, $P < 0.05$) in the hES-EC-injected group was significantly higher compared to that in the saline-injected group. Moreover, the total vascular density in the hES-EC+MC-injected group (14.7 ± 0.6%) was markedly higher compared to those in the other four groups ($P < 0.001$ vs control, $P < 0.01$ vs hES-ECs, $P < 0.05$ vs hES-MCs) (Figure 5C).

Analysis of the infarct size and apoptosis in the ipsilateral side after the transplantation

There was no significant difference in the infarct area in the striatum on day 28 after MCAo between the saline- (1.372 ± 0.041 mm^2: n = 10) and the hMNC- (1.438 ± 0.084 mm^2: n = 10) injected groups. The infarct area in the hES-EC- (1.308 ± 0.094 mm^2: n = 6) or the hES-MC- (1.249 ± 0.047 mm^2: n = 6) injected group showed a tendency to decrease. A significant decrease in the infarct area was observed in the hES-EC+MC-injected group (1.167 ± 0.085 mm^2: n = 9, $P < 0.05$) compared to the saline- and hMNCs-injected groups (Figure 6A, B). We also confined that the infarct volume was significantly reduced in the hES-EC+MC-injected group on day 28 after MCAo, compared to the saline-injected group (hES-EC+MC = 1.475 ± 0.083 mm^3: n = 9, saline = 1.736 ± 0.057 mm^3: n = 11, $P < 0.05$) (Figure 6C). On day 14 after MCAo, the number of ss-DNA$^+$ cells in the ischemic penumbral area in the hES-EC+MC-injected group (17.8 ± 2.5/mm^2: n = 5, $P < 0.05$) significantly decreased compared to that of the saline-injected group (43.5 ± 5.4/mm^2: n = 5) (Figure 6D, E).

Assessment of recovery of impaired motor function after MCAo

We estimated the exercise time by the rota-rod to evaluate the recovery of impaired motor function. Just before the experiment (day0) and on day 7 after MCAo, there was no significant difference of the exercise time in the 5 groups. Even on day 28 after MCAo, significant recovery of impaired motor function was not detected in the hES-EC- (31.2 ± 0.8 seconds, n = 7) or the hES-MC- (30.8 ± 0.7 seconds, n = 7) injected group, compared to that of the saline- (29.5 ± 1.2 seconds, n = 12) or hMNC- (30.1 ± 0.8 seconds, n = 15) injected group. On the other hand, we observed the improvement in the hES-EC+MC-injected group on day 28 after MCAo (33.1 ± 1.3 seconds, n = 13 vs saline or hMNC group: $P < 0.05$) (Figure 6F).

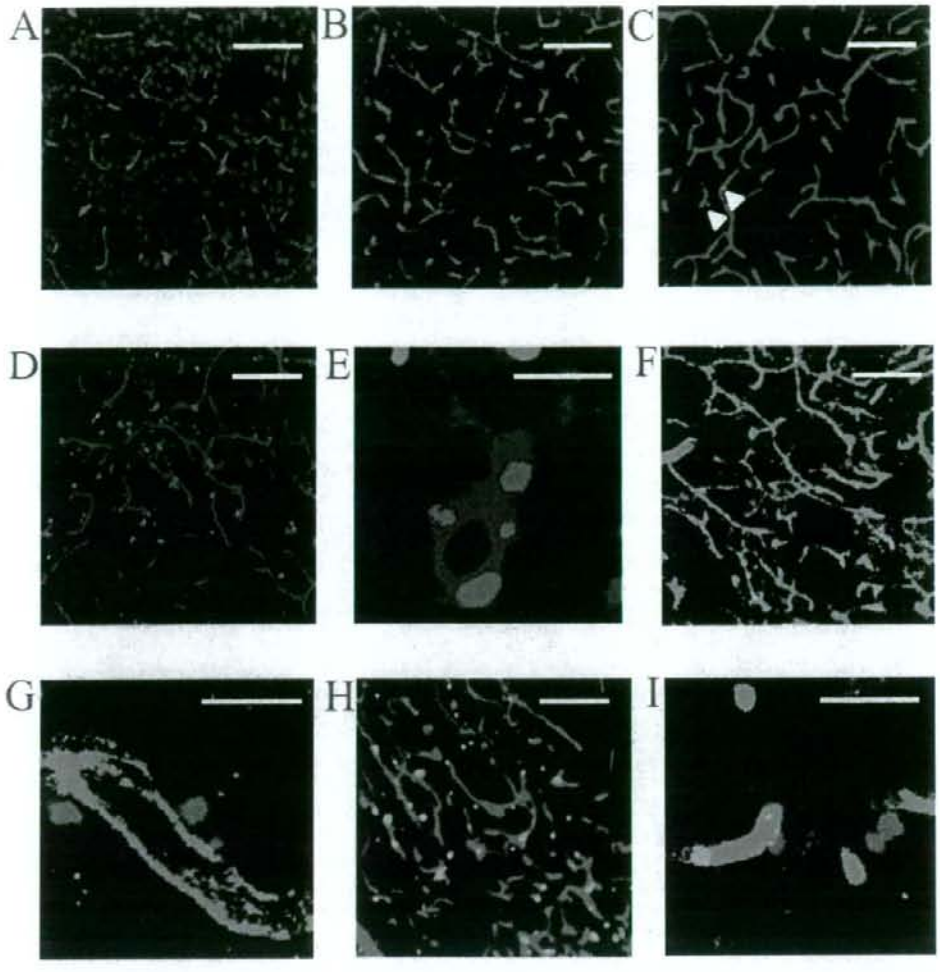

Figure 4 *(see previous page)*
Histological examination of the vasculature in the non-ischemic and ischemic striatum on day 28 after MCAo. A-C: Immunostaining of mouse PECAM-1 (red)/Neu-N (blue) in the non-ischemic striatum (A), and the ischemic striatum in saline (B)-and hMNC (C)-injected mice. Arrows show human PECAM-1$^+$ (green) cells in the ischemic striatum in the hMNC-injected group. D-E: Representative fluorescent photographs of the ischemic striatum stained for mouse PECAM-1 (blue), Neu-N (green) and CM-DiI (red) in hES-EC-injected mice. F-G: Immunostaining of αSMA (blue)/mouse PECAM-1 (green)/human HLA-A,B,C (red) in the ischemic striatum in the hES-MC-injected mice. Human HLA positive and αSMA positive hES-MCs were shown as purple (red+blue) cells. H, Immunostaining of mouse PECAM-1 (red)/Neu-N (blue)/human Pecam-1 (green) in the ischemic striatum in the hES-EC+MC-injected groups. I, Localization of transplanted hES-ECs+MCs in the ischemic striatum stained for αSMA (blue)/mouse PECAM-1 (green)/human HLA-A,B,C (red). A-D/F/H, scale bar: 100 μm, ×20 magnification. E/G/I, scale bar: 20 μm, ×63 magnification.

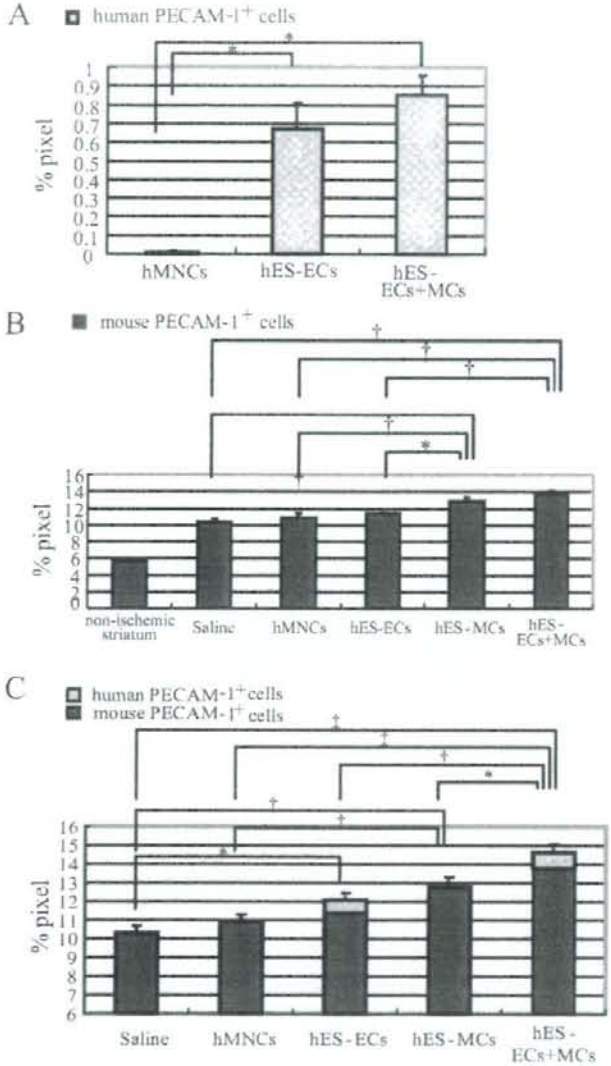

Figure 5

Evaluation of vascular regeneration in the striatum on day 28 after stroke in the five groups. A, Quantification of the density of human PECAM-1+ cells (%area) in the ischemic striatum in hMNC-, hES-EC- and hES-EC+MC-injected groups. * $P < 0.0001$. B, Quantitative analysis of the density of mouse PECAM-1+ cells (%area) in the non-ischemic striatum and in the ischemic striatum in five groups. * $P < 0.05$, † $P < 0.01$. C, Quantification of the total density of human and mouse PECAM-1+ cells (%area) in the ischemic striatum in five groups. * $P < 0.05$, †$P < 0.01$, ‡ $P < 0.001$.

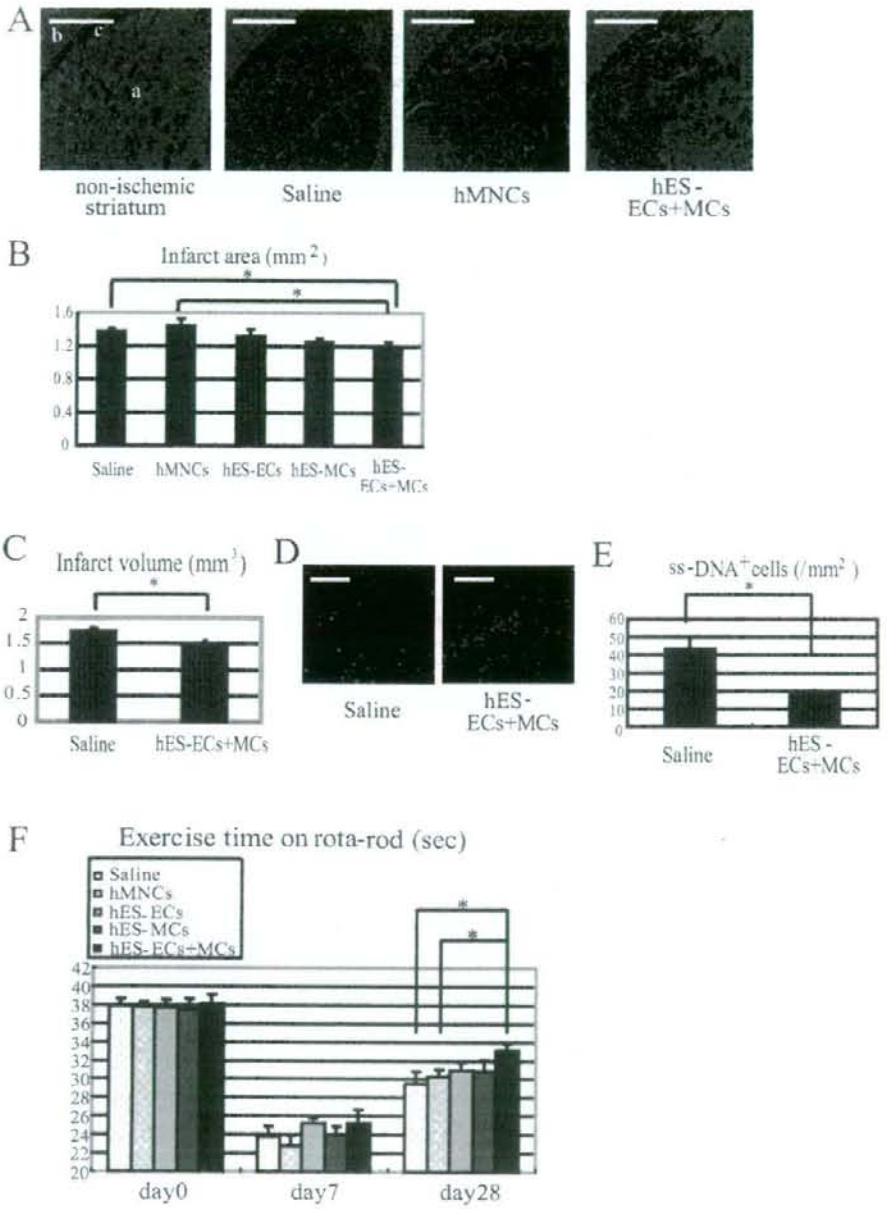

Figure 6 *(see legend on next page)*

Figure 6 *(see previous page)*
Effects of the transplanted cells on neuroprotection and recovery of impaired motor function after MCAo. A-B, Representative fluorescent photograph in non-ischemic and ischemic striatum. a, striatum; b, cortex; c, external capsule. The area where Neu-N expression was lost in the striatum in the saline-, hMNC- and hES-EC+MC-injected group represent the infarct areas (A) (mouse PECAM-1: red, Neu-N: blue. scale bar: 500 μm, ×5 magnification). B-C, Quantitative analysis of the infarct area (5 groups) in the striatum (B) and the infarct volume in the saline- and hES-EC+MC-inejcted group (C) on day 28 after MCAo.* $P < 0.05$. D-E, Representative fluorescent photographs on day 14 after MCAo and quantification of ss-DNA$^+$ cells in the ischemic penumbral area in the saline- and hES-EC+MC-injected group. (ss-DNA: green, Neu-N: blue. Scale bar:100 μm, ×20 magnification. *$P < 0.05$). F, Assessment of recovery of impaired motor function by quantification of the time from the start of the exercise until collapse on an accelerating rota-rod just before the experiments (= day 0) and on day 7 and 28 after MCAo. * $P < 0.05$.

Expression of angiogenic factors in human ES cell derived MCs

We investigated whether the transplanted hES-MCs produced major angiogenic factors such as VEGF, bFGF, HGF and PDGF-BB. Reverse transcription-polymerase chain reaction (RT-PCR) analysis detected mRNA expression of VEGF165, VEGF189, bFGF and HGF in MCs as well as hAoSMCs (Figure 7). In addition, we measured the protein concentration of these angiogenic factors in culture media of hES-MCs by enzyme-linked immunosorbent assay (ELISA). However, the concentration of all factors did not reach the detectable level as follows; the concentration of VEGF, bFGF or HGF was lower than 20 pg/ml, 10 pg/ml, or 0.3 ng/ml.

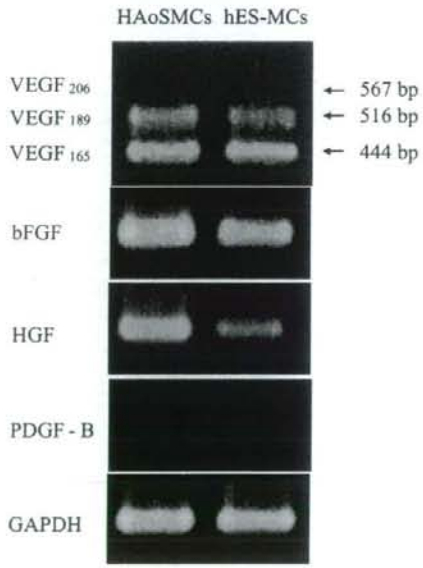

Figure 7
RT-PCR analysis of mRNA expression of VEGF, bFGF, HGF, and PDGF-B in hAoSMCs and hES-MCs. bp indicates base pair.

Discussion

The findings reported here demonstrate that the transplantation of vascular cells, ECs and MCs derived from human ES cells, to the ischemic brain significantly promoted vascular regeneration in the infarct area and consequently contributed to neurological recovery after cerebral ischemia.

It was reported that in animal stroke models, the transplantation of human bone marrow stromal cells, which secrete basic fibroblast growth factor (bFGF) [16] and vascular endothelial growth factor (VEGF) [17], activates the endogenous expression of bFGF, VEGF and VEGFR2, and consequently promotes endogenous angiogenesis, while very few transplanted cells were incorporated into the host circulation [3]. Human CD34$^+$ cells isolated from umbilical cord blood were found to be capable of secreting several angiogenic factors, including VEGF, bFGF and hepatocyte growth factor (HGF) [18] and administration of these CD34$^+$ cells after cerebral ischemia was shown to promote endogenous angiogenesis mainly due to the supply of these angiogenic factors [5]. Bone marrow mononuclear cells containing small number of EPCs participated in neovascularization after focal cerebral ischemia in mice [4] or patients with limb ischemia [19]. However, Rehamn et al. demonstrated that EPCs, which were positive for acLDL and ulex-lectin, have little ability to proliferate and could release several angiogenic growth factors, i.e., VEGF, HGF and G-CSF [20]. Therefore, angiogenic effects induced by the transplantation of EPCs might be partially considered to be attributed to their growth factor secretion.

In contrast, ES cells with pluripotency and self-renewal are highlighted as a promising cell source for regeneration medicine. We have demonstrated that ECs- and MCs-derived from human ES cells could have a high ability of

proliferation and be successfully expanded in large scale for the cell source of therapeutic vasculogenesis.

In the focal stroke model, endogenous angiogenesis in the ischemic area increased partially via the promotion of the expression of VEGF and bFGF in stroke areas [3], and in the present study, the increase of vascular density in saline-injected group on day 28 after MCAo was actually observed. The finding that there was no significant difference in CBF or vascular density between saline- and hMNCs-injected groups indicated that the effects induced by cell transplantation itself, such as the inflammatory reaction or embolic change, may have little or no influence on neovascularization after MCAo. Compared to the saline- or hMNCs-injected groups, CBF in the hES-EC-injected group increased significantly, while no significant increase in the number of mouse PECAM-1 positive cells was observed in the ischemic striatum on day 28 after MCAo. So, we consider that the transplanted hES-ECs detected in host capillaries could participate in neovascularization and make a partial contribution to functional blood vessels.

It is widely considered that during angiogenesis, the recruitment of periendothelial cells (MCs) toward endothelial cells sprouted from host capillaries promotes vascular stabilization and maturation [21-23]. We therefore assume that the increase in endogenous angiogenesis observed in the hES-MC-injected group in our study may have been partially due to a reduction in the retraction of newly-developed endothelial tubes and the promotion of vascular maturation via adequate MC coating.

Recent report demonstrated that endothelial cells derived from rhesus ES cells expressed von Willebrand factor (vWF), CD146 and CD34, but not CD31 and VE-cadherin by flow cytomerty and RT-PCR analyses [24]. Moreover, another report suggested that the cell surface VE-cadherin-negative populations derived during the differentiation procedure to vascular endothelial cells in cynomolgus monkey ES cells, which showed obvious cord-forming capacities and a uniform acetylated low-density lipoprotein (Ac-LDL)-uptaking activity, expressed VE-cadherin intracellularily. In addition, because RT-PCR analysis demonstrated the presence of the VE-cadherin message from the VE-cagherin-negative cells, they considered that these cells might be 'atypical' vascular endothelial cells [25]. Although, by reverse transcription-polymerase chain reaction (RT-PCR) analysis, we examined the mRNA expression of VE-cadherin in the hES-MCs to clarify whether the cell population was consisted of pure MCs or including 'atypical' ECs, the VE-cadherin message of the hES-MCs was not detected [see Additional file 1]. As shown in Figure 2H–I, the morphology of the hES-MCs was similar to hAoSMCs and all of the hES-MCs were positive for markers of mural cells as well as hAoSMCs. In the hES-MC-injected group, moreover, we could detect no human HLA-positive and αSMA-negative cells in the ischemic striatum, especially the host endothelial tubes. Therefore, we consider that the hES-MCs used for the transplantation were really pure MCs but not including 'atypical' ECs, and that the results observed in the hES-MC-injected group were brought by the transplantation of pure MCs itself.

The coordination of these beneficial effects on neovascularization of hES-ECs and hES-MCs could result in the increase in CBF and the marked promotion of vascular density in the ischemic striatum after the transplantation of hES-ECs+MCs. In the hES-EC+MC-injected group, the improvement in CBF was not seen to be as remarkable as that in the vascular density on day 28 after MCAo. Because the blood flow under the MCA, measured in our study, indicates the sum of both that in the ischemic striatum and that in the non-ischemic area, such as the cerebral cortex, we consider that the rate in the rise of CBF in the ipsilateral side might be underestimated.

We demonstrated that in the hES-MCs, RT-PCR analysis detected mRNA expression of some angiogenic factors, such as VEGF, bFGF and HGF, whereas the protein concentration of these factors in culture media was not enough to be detectable. Therefore, we consider that although the secretion of these angiogenic factors might have a possibility to affect the effect of hES-MCs transplantation, adequate MC coating might be more important for the promotion of endogenous angiogenesis after stroke, as observed in the hES-MC- or hES-EC+MC-injected group.

Moreover, in the hES-EC+MC-injected group, significant reduction of apoptotic cells in the ischemic core and infarct volume was observed. Even in a focal stroke model, it was suggested that greater than 80% of newly-formed neurons, which occurs in the subventricular zone of lateral ventricule or in the dentate gyrus of the hippocampus in the adult brain, died, most likely because of unfavorable environmental condition including lack of trophic support and exposure to toxic products from damaged tissues [26,27]. Thus, we assume that the marked promotion of neovascularization as seen in the hES-EC+MC-injected group could provide trophic support and remove toxic products to enhance survival of newly-formed neurons and consequently might promote neuroprotection in the ischemic striatum after stroke.

Conclusion

We have demonstrated that ECs and MCs could be effectively differentiated from human ES cells and expanded on a large scale. Transplantation of these vascular cells

markedly enhanced neovascularization in the ischemic brain and consequently promoted neuroprotection in a transient MCAo model. These finding suggest that vascular cells derived from human ES cells may have a potential to be a source for therapeutic vascular regeneration after stroke.

Abbreviations

ES cells: Embryonic stem cells; VEGF-R2: vascular endothelial growth factor receptor type 2; ECs: endothelial cells; MCs: mural cells; hMNCs: human peripheral blood mononuclear cells; MCAo: middle cerebral artery occlusion; αSMA: alpha smooth muscle actin; hES-ECs+MCs: a mixture of ECs and MCs derived from human ES cells; hES-ECs: ECs derived from human ES cells; hES-MCs: MCs derived from human ES cells.

Competing interests

The authors declare that they have no competing interests.

Authors' contributions

NO wrote the manuscript, performed all experiments, and analyzed data. HI designed and revised the manuscript. MS, KY, DT, and HT participated the maintenance of human ES cell line (HES-3). KM participated the induction of middle cerebral artery occlusion (MCAo) in mice. KP, YF and NT analyzed data and performed statistics. MI and TS participated the maintenance of mice. KN designed and edited the manuscript. All authors read and approved the manuscript.

Additional material

Additional file 1

RT-PCR analysis of mRNA expression of VE-cadherin in hES-MCs, hES-ECs and HUVECs. Total cellular RNA was isolated from hES-MCs, hES-ECs and Human umbilical vein endothelial cells (HUVECs) with RNAeasy Mini Kit (QIAGEN K.K., Tokyo, Japan). The mRNA expression was analyzed with One Step RNA PCR Kit (Takara, Out, Japan). hES-ECs and HUVECs were used for positive controls. An initial 15-minute, 95°C hotstart was used, followed by cycles consisting of 1 minute denaturation at 94°C, 1 minute annealing, and 1 minute extension at 72°C. A 10-minute extension was done at 72°C after the final cycle. Thirty-five cycles were done for VE-cadherin. Oligonucleotide primer sequences, annealing temperature (Ta), and predicted product size of VE-cadherin were as follows; forward: 5'-ACGGGATGACCAAGTACAGC-3', reverse: 5'-ACACACTTTGGGCTGGTAGG-3', Ta: 58°C, product size: 597 base pair. mRNA expression of VE-cadherin was detected in the hES-ECs or HUVECs, but not in the hES-MCs.

Click here for file

[http://www.biomedcentral.com/content/supplementary/1479-5876-6-54-S1.pdf]

Acknowledgements

The human ES cell (HES-3) was provided by ES cell International Pre Ltd, Singapore. This work was supported by grants from Japanese Ministry of Education, Culture, Sports, Science and Technology, Japanese Ministry of Health, Labor and Welfare, University of Kyoto 21st century COE program and Japan Smoking Foundation.

References

1. Kawamata T, Alexis NE, Dietrich WD, Finklestein SP: **Intracisternal basic fibroblast growth factor (bFGF) enhances behavioral recovery following focal cerebral infarction in the rat.** *J Cereb Blood Flow Metab* 1996, **16**:542-547.
2. Zhang ZG, Zhang L, Jiang Q, Zhang R, Davies K, Chopp M: **VEGF enhances angiogenesis and promotes blood-brain barrier leakage in the ischemic brain.** *J Clin Invest* 2000, **106**:829-838.
3. Chen Jieli, Zhang Zheng Gang, Li Yi, Lei Wang, Yong Xu Xian, Subhash Gautam C, Michael Chopp: **Intravenous Administration of Human Bone Marrow Stromal Cells Induces Angiogenesis in the Ischemic Boundary Zone After Stroke in Rat.** *Circulation research* 2003, **92**:692-699.
4. Zheng Zhang Gang, Li Zhang, Jiang Quan, Chopp Michael: **Bone Marrow-Derived Endothelial Progenitor Cells Participate in Cerebral Neovascularization After Focal Cerebral Ischemia in the Adult Mouse.** *Circulation research* 2002, **90**:284-288.
5. Akihiko Taguchi, Toshihiro Soma, Hidekazu Tanaka, Takayoshi Kanda, Hiroyuki Nishimura, Tomohiro Matsuyama: **Administration of CD34+cells after stroke enhances neurogenesis via angiogenesis in a mouse model.** *J Clin Invest* 2004, **114**:330-338.
6. Kalka C, Masuda H, Takahashi T, Kalka-Moll WM, Silver M, Asahara T: **Transplanted of ex vivo expanded endothelial progenitor cells For therapeutic neovascularization.** *Proc Natl Acad Sci USA* 2000, **97**:3422-3427.
7. Peichev M, Naiyer AJ, Pereira D: **Expression of VEGFR-2 and AC133 by circulating human CD34+ cells identifies a population of functional endothelial precursors.** *Blood* 2000, **95**:952-958.
8. Yamashita J, Itoh H, Hirashima M, Ogawa M, Nishikawa S, Yurugi T, Naito M, Nakao K, Nishikawa S: **Flk1-positive cells derived from embryonic stem cells serve as vascular progenitors.** *Nature* 2000, **408**:92-96.
9. Sone M, Itoh H, Yamashita J, Yurugi-Kobayashi T, Suzuki Y, Kondo Y, Nonoguchi A, Sawada N, Yamahara K, Miyashita K, Kwijun P, Oyamada N, Sawada N, Nishikawa S, Nakao K: **Different differentiation kinetics of vascular progenitor cells in primate and mouse embryonic stem cells.** *Circulation* 2003, **107**:2085-2088.
10. Masakatsu Sone, Hiroshi Itoh, Kenichi Yamahara, Jun Yamashita K, Takami Yurugi-Kobayashi, Akane Nonoguchi, Yutaka Suzuki, Ting-Hsing Chao, Naoki Sawada, Yasutomo Fukunaga, Kazutoshi Miyashita, Kwijun Park, Naofumi Oyamada, Naoya Sawada, Daisuke Taura, Naohisa Tamura, Yasushi Kondo, Shinji Nito, Hirofumi Suemori, Norio Nakatsuji, Sin-Ichi Nisikawa, Kazuwa Nakao: **A pathway for differentiation of human embryonic stem cells to vascular cell components and their potential for vascular regeneration.** *Arterioscler Thromb Vasc Biol* 2007, **27**:2127-34.
11. Kazutoshi Miyashita, Hiroshi Itoh, Hiroshi Arai, Takayasu Suganami, Naoki Sawada, Yasutomo Fukunaga, Masakatsu Sone, Kenichi Yamahara, Takami Yurugi-Kobayashi, Kwijun Park, Naofumi Oyamada, Naoya Sawada, Daisuke Taura, Hirokazu Tsujimoto, Ting-Hsing Chao, Naohisa Tamura, Masashi Mukoyama, Kazuwa Nakao: **The Neuroprotective and Vasculo-Neuro-Regenative Roles of Adrenomedullin in Ischemic Brain and Its Therapeutic Potential.** *Endocrinology* 2006, **147(4)**:1642-1653.
12. Teramoto T, Qui J, Plumier JC, Moskowitz MA: **EGF amplifies the replacement of parvalbumin-expressing striatal interneurons after ischemia.** *J Clin Invest* 2003, **111**:1125-1132.
13. Yunjuan Sun, Kunlin Jun, Lin Xie, Jocelyn Childs, Xiao Ou Mao, David A: **VEGF-induced neuroprotection, neurogenesis, and angiogenesis after focal cerebral ischemia.** *J Clin Invest* 2003, **111**:1843-1851.
14. Takao Sakai, Kamin Johnson J, Michihiro Murozono, Keiko Sakai, Marc Magnuson A, Reinhard Fassler: **Plasma fibronectin supports neuronal survival and reduces brain injury following transient focal cerebral ischemia but is not essential for skin-wound healing and hemostasis.** *Nature Medicine* 2001, **7**:324-330.
15. Hunter AJ, Hatcher J, Virley D, Nelson P, Irving E, Parsons AA: **Functional assessment in mice and rats after focal stroke.** *Neuropharmacology* 2000, **39**:806-816.

16. Hamano K, Li TS, Kobayashi T, Kobayashi S, Matsuzaki M, Esato K: **Angiogenesis induced by the implantation of self-bone marrow cells:a new material for therapeutic angiogenesis.** *Cell Trans* 2000, **9**:439-443.
17. Brunner G, Nguyen H, Gabrilove J, Rifkin DB, Wilson EL: **Basic fibroblast growth factor expression in human bone marrow and peripheral blood cells.** *Blood* 1993, **81**:631-638.
18. Marcin Majka, Anna Janowska-Wieczorek, Janina Ratajczak, Karen Ehrenman, Zbigniew Pietrzkowski, Mariusz Ratajczak Z: **Numerous growth factors, cytokines, and chemokines are secreted by human CD34$^+$ cells, myeloblasts, erythroblasts, and megakaryoblasts and regurate normal hematopoiesis in an autocrine/paracrine manner.** *Blood* 2001, **97**:3075-3085.
19. Eriko Tateishi-Yuyama, Hiroaki Matsubara, Toyoaki Murohara, Uichi Ikeda, Satoshi Shintani, Tsutomu Imaizumi: **Therapeutic angiogenesis for patients with limb ischaemia by autologous transplantation of bone-marrow cells: a pilot study and a randomised controlled trial.** *Lancet* 2002, **360**:427-435.
20. Rehman J, Li J, Orschell CM, March KL: **Peripheral blood "endothelial progenitor cells" are derived from monocyte/macrophages and secrete angiogenic growth factors.** *Circulation* 2003, **107**:1164-1169.
21. Asahara Takayuki, Chen Donghui, Takahashi Tomono, Fujikawa Koshi, Kearney Marianne, Jeffrey Isner M: **Tie2 Receptor Ligands, Angiopoietin-1 and Angiopoietin-2, Modulate VEGF-Induced Postnatal Neovascularization.** *Circulation Research* 1998, **83**:233-240.
22. Risaw W: **Mechanism of angiogenesis.** *Nature* 1997, **386**:671-674.
23. Diane Darland C, Patricia D'Amore A: **Blood vessel maturation: vascular development comes of age.** *The Journal of Clinical Investigation* 1999, **103**:157-158.
24. Dan Kaufman S, Rachel Lewis L, Eric Hanson T, Robert Auerbach, Johanna Plendl, James Thomson A: **Functional endothelial cells derived from rhesus monkey embryonic stem cells.** *Blood* 2004, **103**:1325-1332.
25. Saeki K, Yoshiko Y, Nakahara M, Nakamura N, Matsuyama S, Koyanagi A, Yagita H, Koyanagi M, Kondo Y, You A: **Highly efficient and feeder-free production of subculturable vascular endothelial cells from primate embryonic stem cells.** *Journal of Cellular Physiology* 2008, **217**:261-280.
26. Nakatomi H, Kuriu T, Okabe S, Yamamoto S, Hatano O, Nakafuku M: **Regeneration of hippocampal pyramidal neurons after ischemic brain injury by recruitment of endogenous neural progenitors.** *Cell* 2002, **110**:429-441.
27. Arvidsson A, Collin T, Kirik D, Kokaia Z, Lindvall O: **Neuronal replacement from endogenous precursors in the adult brain after stroke.** *Nat Med* 2002, **8**:963-970.

Available online at www.sciencedirect.com
ScienceDirect
Biochemical and Biophysical Research Communications 367 (2008) 840–845
BBRC
www.elsevier.com/locate/ybbrc

cGMP rescues mitochondrial dysfunction induced by glucose and insulin in myocytes

Masanori Mitsuishi, Kazutoshi Miyashita *, Hiroshi Itoh

Department of Internal Medicine, School of Medicine, Keio University, 35 Shinano-machi, Research Park 5N8, Shinjuku-ku, Tokyo 160-8582, Japan

Received 27 December 2007
Available online 14 January 2008

Abstract

Mitochondrial dysfunction in the skeletal muscle has been implicated in a wide variety of pathological processes including insulin resistance in type 2 diabetes. A recent report indicates that calorie restriction can modulate mitochondrial function through the nitric oxide/cGMP-dependent pathway. Following up on these findings, we examined whether cGMP could rescue mitochondrial dysfunction in C2C12 myotubular cells induced by conditions of high-glucose and high-insulin. Treatment of the cells with cGMP promoted mitochondrial biogenesis and ATP synthesis without enhancing production of reactive oxygen species (ROS) in association with up-regulation of the genes involved in oxidative phosphorylation and ROS reduction. The increased mitochondria were revealed to have lower membrane potential, which is similar to the effect of calorie restriction, and reversed mitochondrial dysfunction caused by high-glucose and high-insulin. These results indicated that augmented cGMP-dependent cascades in the skeletal muscle may attenuate insulin resistance observed in patients with type 2 diabetes and metabolic syndrome.

Keywords: cGMP; Mitochondria; Diabetes; Insulin resistance; Skeletal muscle; Mitochondrial biogenesis; Reactive oxygen species; Calorie restriction; PGC1

Mitochondria are energy-producing organelles that generate ATP by means of oxidative phosphorylation (OXPHOS). Impairment of ATP production causes cellular dysfunction, particularly in tissues with higher energy expenditure, including heart, skeletal muscle, and nervous system, and has been implicated in a wide variety of pathological processes including neuro-degeneration, myopathy, obesity, and insulin resistance [1,2].

The number of mitochondria and the rate of ATP synthesis are known to decrease concomitantly in the skeletal muscle of patients with type 2 diabetes mellitus [3,4]. Moreover, offspring of diabetic patients show a reduction in mitochondrial density and ATP production even in the pre-diabetic state [5,6]. Inherited defects in the mitochondrial OXPHOS system in the skeletal muscle are therefore assumed to cause insulin resistance. However, no treatment has been aimed to modulate mitochondrial function to date.

Reactive oxygen species (ROS), which can rapidly impair a wide variety of intracellular molecules including lipids, proteins, and nucleic acids, and thus cause mitochondrial and cellular dysfunction, are also generated as a by-product of ATP [7]. Cumulative cellular damage caused by ROS has been shown to play a central role in the pathogenesis of cardiovascular diseases, cancer and aging [8]. Inappropriate synthesis of ATP with excessive ROS may therefore be harmful for living organisms.

Abbreviations: cGMP, guanosine-3′,5′-cyclic monophosphate; NO, nitric oxide; ATP, adenosine triphosphate; ROS, reactive oxygen species; OXPHOS, oxidative phosphorylation; ATPsyn, ATP synthase; COXIV, cytochrome *c* oxidase complex IV; UCP3, uncoupling protein 3; SOD2, superoxide dismutase 2; PGC1, PPAR gamma coactivator 1; NRF1, nuclear respiratory factor 1; mtTFA, mitochondrial transcription factor A; PPARδ, peroxisome proliferator-activated receptor delta; NFκB, nuclear factor-kappa B; CREB1, CCAAT enhancer-binding protein 1.

* Corresponding author. Fax: +81 3 3354 7446.
E-mail address: miyakaz@sc.itc.keio.ac.jp (K. Miyashita).

0006-291X/$ - see front matter © 2008 Elsevier Inc. All rights reserved.
doi:10.1016/j.bbrc.2008.01.017

A recent report has proposed the notion of "efficient mitochondria" which possess an organized electron transport system that can generate enough ATP, while at the same time maintaining lower oxygen consumption [9]. This study demonstrated that ROS production was reduced in the cells incubated with serum from rats submitted to long term calorie restriction by inducing "efficient mitochondria". Another study found that nitric oxide/cGMP-dependent pathways participate in the modulation of mitochondrial function induced by calorie restriction [10]. However, the exact mechanism for the regulation of mitochondrial function by cGMP has not been identified.

In light of these findings, we explored the roles of cGMP in the regulation of mitochondrial function by using C2C12 myotubular cells and investigated whether cGMP could rescue mitochondrial dysfunction induced by high-glucose and high-insulin, which are generally observed in type 2 diabetes and metabolic syndrome.

Materials and methods

Cell culture. C2C12 cells (RIKEN BioResource Center, Tsukuba, Japan), which were derived from murine skeletal myoblast cells, were grown to confluence in DMEM (Dulbecco's modified Eagle's medium, Gibco, Gaithersburg, MD) supplemented with 10% fetal bovine serum (FBS) and differentiated into myotubes by means of incubation with 0.1% FBS for 7 days. The C2C12-derived myotubes were then treated for 48 h with or without a potent membrane-permeable agonist of cGMP, 8-*para*-chlorophenylthio-guanosine-3',5'-monophosphate (8-*p*CPT-cGMP, 10^{-4}–10^{-3} mol/l, Calbiochem, La Jolla, CA); a competitive antagonist of cGMP, Rp-8-*p*CPT-cGMP (10^{-3} mol/l, Calbiochem); or a nitric oxide (NO)-donor, *S*-nitroso-*N*-acetylpenicillamine (SNAP, 10^{-6} mol/l, Sigma, St. Louis, MO). When we used low-glucose (100 mg/dl) DMEM, the osmolarity was adjusted by mannitol (Sigma) to that of high-glucose (450 mg/dl) DMEM.

Quantification of mitochondrial DNA copy number. Total DNA was extracted with the aid of Qiamp DNA mini kit (Qiagen, Tokyo, Japan) from the C2C12-derived myotubes incubated with or without the agents specified above for 48 h. The mitochondrial DNA copy number was determined by means of quantitative PCR analysis (ABI7500 Real-Time PCR System, Applied Biosystems, Foster City, CA), using specific primers for the mitochondrial DNA encoded 16S ribosomal RNA gene and the nuclear DNA encoded hexokinase 2 gene, as described previously [11]. Results were estimated from the difference in threshold cycle values (delta-C_t) between the mitochondrial gene and the diploid nuclear gene.

Quantification of mitochondrial mass, ROS production, membrane potential, and ATP content. Mitochondrial mass, mitochondrial ROS production, and membrane potential of the C2C12 cells were determined with the aid of fluorescent dyes, MitoTracker Green FM, MitoSOX Red, which can selectively detect mitochondrial ROS, which is a superoxide derived from mitochondria, and Rhodamine 123 (Molecular Probes, Eugene, OR), with the same procedures as described elsewhere [9,12]. To normalize the data, we used Hoechst 33342 (Molecular Probes) for nuclear staining. The value for mitochondrial mass was normalized by that for nuclei, and the value for mitochondrial ROS and membrane potential was normalized by that for mitochondrial density. After the cells were cultured with or without the aforementioned agents for 48 h, they were treated with the dyes for 10 min, and washed twice with warm PBS. The fluorescent intensity was measured with a Wallac ARVO SX multiplate reader (Perkin-Elmer, Norwalk, CT). ATP content of the cells was determined with the chemi-luminescence method (ATP bioluminescence Assay Kit HS II, Roche Diagnostics, Mannheim, Germany).

Microscopic analysis of mitochondria. Sparsely disseminated C2C12 cells (10^3 cells/cm^2) were stained with fluorescent probes as described above, and visualized with a confocal microscope (LSM510; Carl Zeiss, Tokyo, Japan). Images were acquired with a 20× objective lens.

Estimation of gene expressions by real-time PCR. C2C12 myotubes were incubated for 48 h after addition of 10^{-3} mol/l cGMP. Total RNA was extracted with the aid of an RNeasy Mini kit (Qiagen) according to the manufacturer's instructions. Reverse transcription with an ExScript RT reagent kit (TaKaRa Bio, Otsu, Japan) was performed using 100 ng of the total RNA with oligo-dT as a primer. The level of gene expression was determined by means of quantitative PCRs (ABI 7500) in the presence of a fluorescent dye (SYBR Premix Ex Taq; TaKaRa Bio). The relative quantity of mRNA was calculated after normalization to that of the internal control, 18S gene. Details of the primers (TaKaRa-Bio) used in this study are available on the manufacturer's homepage (http://www.takara-bio.com).

Quantification of protein levels by Western blotting. Total protein (10 μg) from whole cell extracts were stained with antibodies against ATP synthase (1:2000, subunit α, A21350; Molecular Probes), COXIV (1:1000, subunit IV, A21348; Molecular Probes), SOD2 (1:2000, sc-30080; Santa Cruz Biotechnology, Santa Cruz, CA), UCP3 (1:1000, ab3477; Abcam plc, Cambridge, UK) and beta-actin (1:1000, #4967; Cell Signaling, Danvers, MA). Proteins were separated by means of SDS–PAGE (Bio-Rad Laboratories, Hercules, CA), transferred to nitrocellulose membranes after electrophoresis, and incubated with the corresponding antibodies for 12–48 h at 4 °C. Membranes were probed with their secondary antibodies labeled with horseradish peroxidase (1:3000–1:10,000). Immuno-labeled proteins were detected by using a chemi-luminescence kit (ECL Plus; GE Healthcare, Tokyo, Japan) and a lumino-image analyzer (LAS-3000; FujiFilm, Tokyo, Japan). The density of the blot for each protein relative to that for the internal control, beta-actin, was also estimated by means of imaging software (MultiGauge; FujiFilm).

Statistical analysis. All data were expressed as means ± standard error. Comparison of means between two groups was performed with Student's *t* test. When more than two groups were compared, analysis of variance was used to evaluate significant differences among groups, and if significant differences were confirmed, each difference was further examined by means of multiple comparisons. p value < 0.05 was considered to be statistically significant.

Results

cGMP promotes mitochondrial biogenesis and ATP synthesis without enhancing ROS generation in C2C12 myotubes

To investigate the effects of cGMP on mitochondrial biogenesis and ROS production, we incubated C2C12 myotubular cells for 48 h with or without 10^{-4}–10^{-3} mol/l cGMP. Mitochondrial DNA copy number estimated by means of quantitative PCR analysis showed a significant increase (55% increase at 10^{-3} mol/l, $n = 6$, $p < 0.01$, Fig. 1A) in parallel with the increase in cellular ATP content (Fig. 1B). Mitochondrial density estimated by means of fluorescent staining demonstrated a dose-dependent increase induced by cGMP (Fig. 1C). In spite of the increase in mitochondrial mass, mitochondrial ROS showed a significant decrease (17% decrease at 10^{-3} mol/l, $n = 12$, $p < 0.01$, Fig. 1C) when the value was normalized by the mitochondrial mass. The increase in mitochondria induced by a representative NO-donor, *S*-nitroso-*N*-acetylpenicillamine (SNAP, 10^{-6} mol/l) was similar to that induced by cGMP; however, ROS production per mitochondria remained unchanged at least 48 h after the treatment (Fig. 1C). Microscopic analysis with a confocal

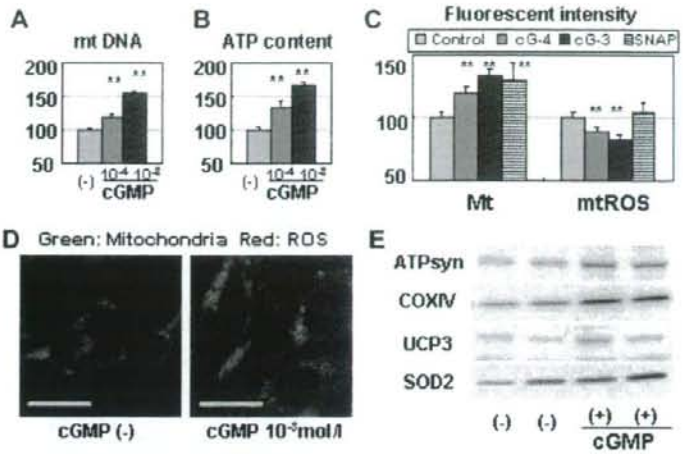

Fig. 1. cGMP promotes mitochondrial biogenesis and ATP synthesis without enhancing ROS production in C2C12 myotubes. C2C12 cells were incubated with or without cGMP (8-*p*CPT-cGMP, at the concentrations indicated: 10^{-4}–10^{-3} mol/l) or SNAP (10^{-6} mol/l) for 48 h. (A) Mitochondrial DNA copy number (mtDNA) estimated by quantitative PCR analysis ($n = 6$ per group). (B) ATP content determined with the chemi-luminescence method ($n = 6$). (C) Mitochondrial density (Mt) and mitochondrial ROS production (mtROS) estimated with the aids of fluorescent probes ($n = 12$). cG-4, treatment with cGMP 10^{-4} mol/l; cG-3, with cGMP 10^{-3} mol/l; SNAP, with SNAP 10^{-6} mol/l. (D) Mitochondrial mass (green) and mitochondrial ROS (red) were visualized by means of fluorescent probes and confocal microscopy after incubation for 48 h with or without cGMP (10^{-3} mol/l). Scale bar: 100 μm. (E) Western blot analysis of protein levels that play significant roles in ATP production and ROS reduction. C2C12 myotubes were treated with or without cGMP (10^{-3} mol/l) for 48 h. ATPsyn, ATP synthase; COXIV, cytochrome *c* oxidase complex IV; UCP3, uncoupling protein 3; SOD 2, superoxide dismutase 2. The values were standardized to those of control. $^{**}p < 0.01$ compared to control. (For interpretation of color mentioned in this figure the reader is referred to the web version of the article.)

microscope confirmed the result by visualization of the C2C12 cells treated with cGMP that had accumulated more mitochondrial (green) and fewer ROS (red) probes (Fig. 1D). Promotion of ATP production by cGMP was further confirmed by Western blot, which showed increases in ATP synthase and COXIV protein levels when cGMP was added to the culture medium (Fig. 1E). In addition, UCP3 and SOD2, which are known to contribute to ROS reduction, also increased as a result of the addition of cGMP (Fig. 1E).

cGMP augments expressions of genes participating in mitochondrial biogenesis, ATP production and ROS reduction

Mitochondrial DNA copy number after the treatment with cGMP (10^{-3} mol/l) started to increase at 6 h and continued to increase at least for 48 h (Fig. 2A). After the addition of cGMP; we examined the time course of expressions of genes that were known to have been involved in mitochondrial biogenesis (PGC1α, PGC1β, NRF1, and mtTFA), oxidative phosphorylation (ATP synthase and COXIV) and ROS reduction (UCP3 and SOD2) at various time points (6, 24, and 48 h), and found that gene expressions of ATP synthase, COXIV, UCP3, and SOD2 had significantly increased after 6 h (Fig. 2B). These increases were maintained for 24 h, but 48 h after the treatment, most of the expression levels had returned to basal values. In subsequent experiments, we estimated the effect of cGMP on the up-stream genes for mitochondrial biogenesis, namely, PGC1α, PGC1β, NRF1, and mtTFA, which positively regulate it. These gene expressions had increased synchronously increased 6 h after the addition of cGMP and returned to basal levels after 48 h, so that the time course was parallel to that for ATP synthase and COXIV (Fig. 2C). We also checked the effect of cGMP on the gene expressions of positive regulator for UCP3 (MyoD and PPARδ) and SOD2 (NFκB and CREB1). These expressions of PPARδ and CREB1 were up-regulated by cGMP and returned to basal level 48 h after the addition (Fig. 2D). However, the gene expressions of MyoD and NFκB showed no significant increase in response to cGMP (Fig. 2D).

cGMP rescues mitochondrial dysfunction caused by high-glucose and high-insulin in C2C12 myotubes

To examine the influence on mitochondrial function of high-glucose and high-insulin exposure that is generally seen in type 2 diabetic patients, we checked the effect of glucose and insulin on mitochondrial density, ROS production and membrane potential in C2C12 cells. High-glucose (450 mg/dl) significantly reduced mitochondria content in comparison with the reduction induced by low-glucose (100 mg/dl), while significant increase was observed in mitochondrial ROS production and higher membrane

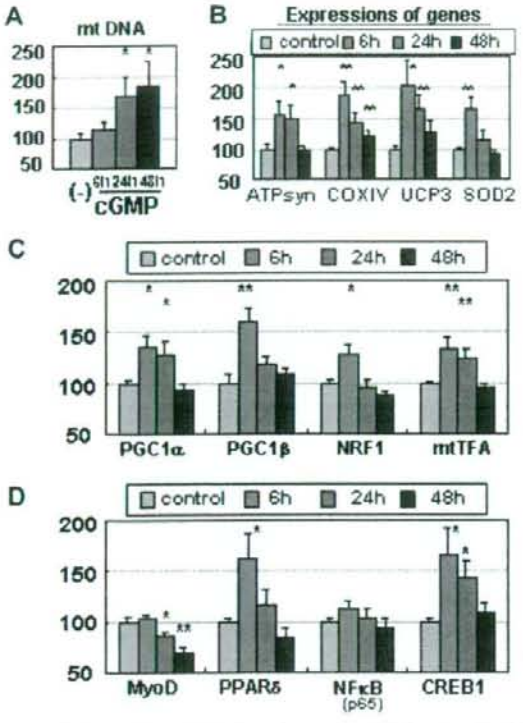

Fig. 2. cGMP augments expressions of genes involved in mitochondrial biogenesis, ATP production and ROS reduction. C2C12 cells were incubated with cGMP (10^{-3} mol/l) and harvested at various time points (6, 24, and 48 h after the addition of cGMP) for gene expression analysis by quantitative PCR. (A) Time course of augmentation of mitochondrial DNA copy number (mtDNA) after addition of cGMP ($n = 6$ per group). (B) Quantitative PCR analysis of gene expressions involved in ATP production and ROS reduction ($n = 8$). (C) Expression of genes involved in mitochondrial biogenesis ($n = 8$). (D) Expression of genes involved in the regulation of UCP3 (MyoD and PPARδ) or SOD2 (NFκB and CREB1) ($n = 8$). PGC1, PPAR gamma coactivator 1; NRF1, nuclear respiratory factor 1; mtTFA, mitochondrial transcription factor A; PPARδ, peroxisome proliferator-activated receptor delta; NFκB, nuclear factor-kappa B (subunit p65); CREB1, CCAAT enhancer-binding protein 1. The gene expressions were normalized by that of the internal control (18S gene). The values were standardized to those of control. $^{*}p < 0.05$, $^{**}p < 0.01$ compared to control.

potential (Fig. 3A). On the other hand, treatment with insulin significantly increased mitochondrial ROS production and membrane potential, without causing significant change in mitochondrial mass (Fig. 3B). The combination of high-glucose and high-insulin reduced the mitochondrial mass in association with a significant increase in mitochondrial ROS production and membrane potential (Fig. 3C). Treatment with cGMP significantly increased mitochondrial density which had decreased under conditions of high-glucose and high-insulin condition, accompanied by a reduction in mitochondrial ROS production and membrane potential (Fig. 3C). These effects of cGMP were almost completely nullified by the cGMP antagonist (Fig. 3C). Western blot analysis disclosed that protein levels for ATP synthase, COXIV, UCP3, and SOD2 had concurrently decreased under high-glucose and high-insulin conditions (Fig. 3D). As with mitochondrial density, cGMP reversed the decrease in protein levels and the cGMP antagonist nullified the effect (Fig. 3D). These results were confirmed by the densitometry of Western blots (Fig. 3E).

Discussion

In the study presented here, we found that cGMP increased mitochondrial density in cultured C2C12 myotubes combined with lower membrane potential and ROS production, which was similar to the result that obtained with calorie restriction. cGMP also reversed the mitochondrial dysfunction caused by high-glucose and high-insulin. The quantitative PCR analysis demonstrated that the treatment with cGMP induced expression of genes participating in mitochondrial biogenesis and oxidative phosphorylation, including PGC1α, NRF1, ATP synthase, and COX-IV, accompanied with those contributing to ROS reduction, including UCP3 and SOD2, and their up-stream regulator, PPARδ and CREB1.

A recent study found that calorie restriction induces a large number of efficient mitochondria that could generate enough ATP keeping lower oxygen consumption and ROS production [9]. It was suggested that these functional changes in mitochondrial bioenergetics, which were brought by calorie restriction, are closely related to a reduction in aging and age-related disorders including atherosclerosis, cancer, and diabetes. A characteristic feature of these efficient mitochondria was a reduction in mitochondrial membrane potential, which is the principal parameter regulating generation of mitochondrial ROS [13]. In our study, the treatment of C2C12 myotubes with cGMP produced similar changes in mitochondria, that is, it led to an increase in the number of low-potential mitochondria and thus attained enhancement of ATP content with relative reduction of ROS. On the other hand, a NO-donor SNAP increased mitochondrial density; however, ROS production was not reduced.

We therefore wondered whether cGMP could recover mitochondrial dysfunction caused by high-glucose and high-insulin, a condition which is often seen in diabetic patients. Among a number of mechanisms that have been implicated in functional and morphological changes in mitochondria in diabetic muscle, it has been indicated that a reduction in the expression of key enzymes in mitochondrial biogenesis and oxidative metabolism, including PGC1α, NRF1, ATP synthase, and COXIV, and a subsequent decrease in mitochondrial number and ATP production are essential for the pathogenesis of insulin resistance [14–16]. In addition, a decrease in the antioxidant system, including UCP3 and SOD2, and subsequent augmentation of mitochondrial ROS

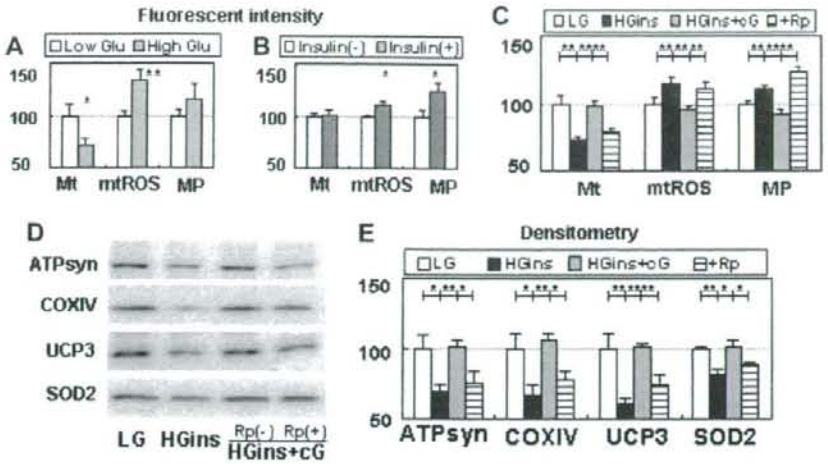

Fig. 3. cGMP rescues mitochondrial dysfunction caused by high-glucose and high-insulin. C2C12 cells were incubated in low-glucose (100 mg/dl), high-glucose (450 mg/dl) or high-glucose plus insulin (100 ng/ml) for 48 h; with or without cGMP (10^{-3} mol/l) or cGMP plus the cGMP-antagonist, Rp-8-*p*CPT-cGMP (10^{-3} mol/l). (A–C) Mitochondrial density (Mt), mitochondrial ROS production (mtROS), and mitochondrial membrane potential (MP) were estimated with the aid of fluorescent probes after incubation for 48 h under the conditions indicated. (A) Low glu, cells were incubated in low-glucose (100 mg/dl) medium; high glu, high-glucose (450 mg/dl) medium ($n = 8$). (B) Insulin (−), cells were incubated in high-glucose medium without insulin; insulin (+), high-glucose medium with insulin ($n = 8$). (C) LG, cells were incubated in low-glucose medium; HGins, high-glucose medium with insulin; HGins+cG, high-glucose medium with insulin plus cGMP (10^{-3} mol/l); Rp, the cGMP antagonist; Rp-8-*p*CPT-cGMP (10^{-3} mol/l) was added to HGins+cG ($n = 12$). (D) Western blot analysis of protein levels of ATP synthase (ATPsyn), cytochrome *c* oxidase complex IV (COXIV), uncoupling protein 3 (UCP3) and superoxide dismutase 2 (SOD2) in the cells incubated under the conditions indicated that were identical to those described for (C). (E) Densitometric analysis of Western blot. The density of the blot for each protein was estimated relative to that for the internal control (beta-actin) ($n = 4$). The values were standardized to those of control. $^{*}p < 0.05$, $^{**}p < 0.01$ compared to control.

are considered to be related to insulin resistance [17]. A reduction in the UCP3 content of the skeletal muscle of pre-diabetic and diabetic patients has been reported and this may account for an increase in mitochondrial membrane potential and subsequent ROS production in diabetic muscle because UCP3 reduces the membrane potential and mitochondrial ROS production [18,19]. Moreover, it has been demonstrated that SOD2, which is a representative molecule of the mitochondrial antioxidant system, is also down-regulated in diabetes [20].

In the study reported here, the combination of high-glucose and high-insulin reduced the mitochondrial mass in association with a significant increase in mitochondrial ROS and membrane potential. These changes were compatible with previously reported findings described above. Concomitant reductions in the protein levels of ATP synthase, COXIV, UCP3, and SOD2 indicated that high-glucose and high-insulin condition had a diminishing effect on not only mitochondrial biogenesis but also the ROS reduction system in mitochondria. In addition, we found that the response of mitochondria to glucose and insulin was similar, but showed certain differences. Glucose strongly reduced mitochondrial mass and insulin significantly increased mitochondrial potential, while both stimuli produced an increase in mitochondrial ROS. High-glucose and high-insulin thus reduced the number of mitochondria and increased membrane potential and ROS production. However, the treatment of C2C12 cells with cGMP increased the number of mitochondria with lower membrane potential but without enhancing ROS production. In accordance with these changes, the protein levels of ATP synthase, COXIV, UCP3, and SOD2 were concomitantly recovered by cGMP and this effect was nullified by cGMP antagonist. These findings suggest that cGMP can rescue mitochondrial dysfunction associated with over-nutrition, a result similar to that induced by calorie restriction.

In summary, the findings in our study demonstrate that cGMP can enhance mitochondrial biogenesis and ATP synthesis in cultured C2C12 myotubes while maintaining lower ROS production in a manner similar to that observed in calorie restriction. The treatment that augments cGMP-dependent signal cascades in the skeletal muscle may therefore attenuate the mitochondrial dysfunction that is observed in type 2 diabetes and metabolic syndrome.

References

[1] D.C. Wallace, Mitochondrial diseases in man and mouse, Science 283 (1999) 1482–1485.
[2] B.B. Lowell, G.I. Shulman, Mitochondrial dysfunction and type b2 diabetes, Science 307 (2005) 384–387.

[3] D.E. Kelley, J. He, E.V. Menshikova, V.B. Ritov, Dysfunction of mitochondria in human skeletal muscle in type 2 diabetes, Diabetes 51 (2002) 2944–2950.
[4] V.B. Ritov, E.V. Menshikova, J. He, R.E. Ferrell, B.H. Goodpaster, D.E. Kelley, Deficiency of subsarcolemmal mitochondria in obesity and type 2 diabetes, Diabetes 54 (2005) 8–14.
[5] K.F. Petersen, S. Dufour, D. Befroy, R. Garcia, G.I. Shulman, Impaired mitochondrial activity in the insulin-resistant offspring of patients with type 2 diabetes, N. Engl. J. Med. 350 (2004) 664–671.
[6] D.E. Befroy, K.F. Petersen, S. Dufour, G.F. Mason, R.A. de Graaf, D.L. Rothman, G.I. Shulman, Impaired mitochondrial substrate oxidation in muscle of insulin-resistant offspring of type 2 diabetic patients, Diabetes 56 (2007) 1376–1381.
[7] S. Melov, Mitochondrial oxidative stress. Physiologic consequences and potential for a role in aging, Ann. N. Y. Acad. Sci. 908 (2000) 219–225.
[8] R.S. Balaban, S. Nemoto, T. Finkel, Mitochondria, oxidants, and aging, Cell 120 (2005) 483–495.
[9] G. López-Lluch, N. Hunt, B. Jones, M. Zhu, H. Jamieson, S. Hilmer, M.V. Cascajo, J. Allard, D.K. Ingram, P. Navas, R. de Cabo, Calorie restriction induces mitochondrial biogenesis and bioenergetic efficiency, Proc. Natl. Acad. Sci. USA 103 (2006) 1768–1773.
[10] E. Nisoli, C. Tonello, A. Cardile, V. Cozzi, R. Bracale, L. Tedesco, S. Falcone, A. Valerio, O. Cantoni, E. Clementi, S. Moncada, M.O. Carruba, Calorie restriction promotes mitochondrial biogenesis by inducing the expression of eNOS, Science 310 (2005) 314–317.
[11] M. Lagouge, C. Argmann, Z. Gerhart-Hines, H. Meziane, C. Lerin, F. Daussin, N. Messadeq, J. Milne, P. Lambert, P. Elliott, B. Geny, M. Laakso, P. Puigserver, J. Auwerx, Resveratrol improves mitochondrial function and protects against metabolic disease by activating SIRT1 and PGC-1alpha, Cell 127 (2006) 1109–1122.
[12] A.E. Civitarese, B. Ukropcova, S. Carling, M. Hulver, R.A. DeFronzo, L. Mandarino, E. Ravussin, S.R. Smith, Role of adiponectin in human skeletal muscle bioenergetics, Cell Metab. 4 (2006) 75–87.
[13] D.G. Nicholls, Mitochondrial membrane potential and aging, Aging Cell 3 (2004) 35–40.
[14] V.K. Mootha, C.M. Lindgren, K.F. Eriksson, A. Subramanian, S. Sihag, J. Lehar, P. Puigserver, E. Carlsson, M. Ridderstråle, E. Laurila, N. Houstis, M.J. Daly, N. Patterson, J.P. Mesirov, T.R. Golub, P. Tamayo, B. Spiegelman, E.S. Lander, J.N. Hirschhorn, D. Altshuler, L.C. Groop, PGC-1alpha-responsive genes involved in oxidative phosphorylation are coordinately downregulated in human diabetes, Nat. Genet. 34 (2003) 267–273.
[15] M.E. Patti, A.J. Butte, S. Crunkhorn, K. Cusi, R. Berria, S. Kashyap, Y. Miyazaki, I. Kohane, M. Costello, R. Saccone, E.J. Landaker, A.B. Goldfine, E. Mun, R. DeFronzo, J. Finlayson, C.R. Kahn, L.J. Mandarino, Coordinated reduction of genes of oxidative metabolism in humans with insulin resistance and diabetes: potential role of PGC1 and NRF1, Proc. Natl. Acad. Sci. USA 100 (14) (2003) 8466–8471.
[16] K. Højlund, K. Wrzesinski, P.M. Larsen, S.J. Fey, P. Roepstorff, A. Handberg, F. Dela, J. Vinten, J.G. McCormack, C. Reynet, H. Beck-Nielsen, Proteome analysis reveals phosphorylation of ATP synthase beta-subunit in human skeletal muscle and proteins with potential roles in type 2 diabetes, J. Biol. Chem. 278 (2003) 10436–10442.
[17] A.P. Rolo, C.M. Palmeira, Diabetes and mitochondrial function: role of hyperglycemia and oxidative stress, Toxicol. Appl. Pharmacol. 212 (2006) 167–178.
[18] A.J. Vidal-Puig, D. Grujic, C.Y. Zhang, T. Hagen, O. Boss, Y. Ido, A. Szczepanik, J. Wade, V. Mootha, R. Cortright, D.M. Muoio, B.B. Lowell, Energy metabolism in uncoupling protein 3 gene knockout mice, J. Biol. Chem. 275 (2000) 16258–16266.
[19] C. García-Martínez, B. Sibille, G. Solanes, C. Darimont, K. Macé, F. Villarroya, A.M. Gómez-Foix, Overexpression of UCP3 in cultured human muscle lowers mitochondrial membrane potential, raises ATP/ADP ratio, and favors fatty acid vs. glucose oxidation, FASEB J. 15 (2001) 2033–2035.
[20] R.A. Kowluru, L. Atasi, Y.S. Ho, Role of mitochondrial superoxide dismutase in the development of diabetic retinopathy, Invest. Ophthalmol. Vis. Sci. 47 (2006) 1594–1599.

0013-7227/08/$15.00/0
Printed in U.S.A.

Endocrinology 149(2):483–491
Copyright © 2008 by The Endocrine Society
doi: 10.1210/en.2007-1094

Therapeutic Potential of Atrial Natriuretic Peptide Administration on Peripheral Arterial Diseases

Kwijun Park, Hiroshi Itoh, Kenichi Yamahara, Masakatsu Sone, Kazutoshi Miyashita, Naofumi Oyamada, Naoya Sawada, Daisuke Taura, Megumi Inuzuka, Takuhiro Sonoyama, Hirokazu Tsujimoto, Yasutomo Fukunaga, Naohisa Tamura, and Kazuwa Nakao

Department of Medicine and Clinical Science, Kyoto University Graduate School of Medicine, Kyoto 606-8507, Japan

Peripheral arterial diseases are caused by arterial sclerosis and impaired collateral vessel formation, which are exacerbated by diabetes, often leading to leg amputation. We have reported that an activation of the natriuretic peptides/cGMP/cGMP-dependent protein kinase pathway accelerated vascular regeneration and blood flow recovery in murine legs, for which ischemia had been induced by a femoral arterial ligation as a model for peripheral arterial diseases. In this study, ip injection of carperitide, a human recombinant atrial natriuretic peptide, accelerated blood flow recovery with increasing capillary density in ischemic legs not only in nondiabetic mice but also in mice kept upon streptozotocin-induced hyperglycemia for 16 wk, which significantly impaired the blood flow recovery compared with nondiabetic mice. Based on these findings, we tried to apply the administration of carperitide to the treatment of peripheral arterial diseases. The study group comprised a continuous series of 13 patients with peripheral arterial diseases (Fontaine's classification I, one; II, five; III, two; and IV, five), for whom conventional therapies had not accomplished appreciable results. Carperitide was administrated continuously and intravenously for 2 wk to Fontaine's class I–III patients and for 4 weeks to class IV patients. The dose was gradually increased to the maximum, with the patient's systolic blood pressure being kept above 100 mm Hg. Carperitide administration improved the ankle-brachial pressure index, intermittent claudication, rest pain, and ulcers. In conclusion, this study showed a therapeutic potential of carperitide to treat peripheral arterial diseases refractory to conventional therapies. (*Endocrinology* 149: 483–491, 2008)

LOWER EXTREMITY PERIPHERAL artery disease (PAD), which consists of arteriosclerosis thrombosis and thromboangitis obliterans, is caused by the altered structure and function of the arteries that supply the lower limbs. Numerous pathophysiological processes can contribute to the creation of stenoses or aneurysms of peripheral artery circulation. Among them, diabetes mellitus is one of the most important causes of PAD. According to the Centers for Disease Control and Prevention's National Center for Chronic Disease Prevention and Health Promotion, 82,000 people have diabetes-related leg, foot, or toe amputations each year in the United States. World Diabetes Day announced that up to 70% of leg amputation cases are patients with diabetes. In PAD patients with diabetes, collateral vessel formation is impaired (1), and intricately modified angiogenesis contributes to a large variety of complications including diabetic gangrene (2). Mechanisms that alter angiogenesis in diabetes are largely unknown. It is reported, however, that either inappropriate production or action of nitric oxide (NO) may play important roles in vascular insufficiencies with diabetes (3). NO activates soluble guanylyl cyclase (GC) followed by the cGMP signal transduction cascade (4). Significant reverse correlation between the urinary cGMP excretion rate and the disease grade according to Fontaine's classification observed in PAD patients seems to imply the impact of diminished cGMP production in PAD (5).

Natriuretic peptides (NPs) consist of atrial NP (ANP), brain NP (BNP), and C-type NP (CNP) and elicit various biological effects by activating particulate GCs: GC-A is a receptor selective for ANP and BNP, and GC-B is a receptor selective for CNP (4, 6–8). One of the major mediators of cGMP signaling is cGMP-dependent protein kinase (cGK) (4). ANP and BNP are secreted mainly from the atrium and ventricle of the heart, respectively, and act as cardiac hormones (4, 6, 7). The clinical significance of NPs is already recognized in the diagnosis and treatment of congestive heart failure (CHF). Recombinant human ANP and BNP are used for treating CHF, with the main expectation of diuretic and natriuretic effects (9, 10).

Recently, NPs have been revealed to have various effects on cell survival, proliferation, and differentiation. We reported that ANP at a physiological concentration induces endothelial regeneration in the human coronary artery and umbilical vein through the activation of ERK and phosphatidylinositol 3-kinase/Akt pathways (11). We used genetically engineered mice that overexpress BNP and type I cGK (cGKI), or otherwise lack cGKI, and demonstrated that BNP can promote vascular regeneration and accelerate the restoration of blood flow after the removal of a hind-limb artery in mice through the activation of the GC-A/cGMP/cGKI

First Published Online November 8, 2007

Abbreviations: ABI, Ankle-brachial pressure index; ADMA, asymmetric dimethylarginine; ANP, atrial natriuretic peptide; BNP, brain natriuretic peptide; cGK, cGMP-dependent protein kinase; cGKI, type I cGMP-dependent protein kinase; CHF, congestive heart failure; CNP, C-type natriuretic peptide; EC, endothelial cell; ESRD, end-stage renal disease; GC, guanylyl cyclase; NP, natriuretic peptide; PECAM, platelet endothelial cell adhesion molecule-1; SMC, smooth muscle cell; STZ, streptozotocin; VEGF, vascular endothelial growth factor.

***Endocrinology* is published monthly by The Endocrine Society (http://www.endo-society.org), the foremost professional society serving the endocrine community.**

pathway (12–14). Meanwhile, CNP, which is secreted from endothelial cells (ECs) and acts as an endothelium-derived relaxing peptide (15), also induces redifferentiation of vascular smooth muscle cells (SMCs) while accelerating reendothelialization and suppressing neointimal hyperplasia in vein grafting or balloon injuries in rabbits, which simulate atherosclerotic lesions in humans (16, 17). These observations indicate that GC-A/cGMP and GC-B/cGMP signaling cascades have potential to promote vascular regeneration in PAD and to inhibit the progression of atherosclerotic lesions. On the other hand, we have reported previously that endothelial CNP expression is progressively reduced in accordance with the severity of human coronary atherosclerosis (18), which indicates that not only NO/soluble GC/cGMP signaling but also CNP/GC-B/cGMP signaling might be impaired in PAD. Therefore, the restoration of intracellular cGMP levels by the activation of GC-A, the third signaling pathway using cGMP as the second messenger in vascular SMCs and ECs, could improve PAD.

In this context, we hypothesized that an administration of ANP or BNP could, at least partly, compensate for impaired angiogenesis due to diminished intracellular cGMP levels in PAD patients by an activation of GC-A. In Japan, carperitide, a recombinant human ANP, is already approved and widely used for the treatment of CHF. By contrast, nesiritide, a recombinant human BNP, has not been approved in Japan, and it cannot be applied to rodent models because amino acid sequences and molecular forms of BNP are quite different between humans and rodents. In the present study, we therefore examined the effect of carperitide on vascular regeneration in animal models with diabetes, and we further tried to determine safety and to investigate any possible therapeutic effects of carperitide in PAD patients.

Materials and Methods

Animals

C57BL/6 male mice (CLEA Japan, Inc., Tokyo, Japan) were used for experiments. Diabetes was induced in the mice by repetitive (once a day for 4–6 consecutive days) ip injections of streptozotocin (STZ) (Nacalai Tesque Inc, Kyoto, Japan; 65–100 mg/kg body weight in 200 μl of 10 mM sodium citrate buffer, pH 4.0) at 8 wk of age. Blood glucose concentrations were monitored weekly after STZ treatment with Dexter-ZII (Bayer Medical Ltd., Tokyo, Japan). Animals with blood glucose levels above 220 mg/dl at 2 wk after the first STZ injection were used as STZ-diabetic mice. Control mice received an equal volume of citrate buffer. Mice were used for experiments of limb ischemia at 4, 16, and 26 wk after the first injection of STZ or vehicle.

An animal model of limb ischemia was made by a ligation of one femoral artery. The blood flow in both legs was assessed with a laser Doppler perfusion image analyzer (Moor Instruments, Devon, UK), and the blood flow recovery was assessed by the ischemic limb to normal limb ratio of blood flow, as we described previously (14).

To assess the effect of carperitide, a recombinant human ANP (Daiichi Asubio Pharma Co., Ltd., Tokyo, Japan), on angiogenesis in ischemic limbs, the femoral artery ligation was carried out at 16 wk after the first injection of STZ or vehicle, and carperitide at a dose of 2.2 μg/kg·min or equal volume of water (vehicle) was administered continuously and ip via a microosmotic pump (Alzet model 1002D; Alzet Pharmaceuticals, Palo Alto, CA), which was implanted ip at 3 d after the femoral artery ligation. Pumps were renewed at d 14 after primary implantation. At 28 d from the femoral artery ligation, mice were euthanized by an overdose of pentobarbital injection, and the ischemic hind limb was isolated for the histological analysis.

All experimental procedures were performed according to Kyoto University standards for animal care.

Histological analysis

After fixation with 4% paraformaldehyde, ischemic lower legs were embedded in OCT compound (Sakura Finetechnical, Tokyo, Japan) and frozen at −80 C. Cryostat sections (4–8 μm thick) of the tissue were stained with a rat antimouse platelet EC adhesion molecule-1 (PECAM-1) antibody (item 553370; PharMingen, San Diego, CA). Four random fields on two different sections (3 mm apart) from each mouse were photographed with a digital camera (Olympus, Tokyo, Japan). By computer-assisted analysis using NIH IMAGE, capillary density was calculated as the mean number of capillaries stained with PECAM-1, as we described previously (14).

Patients

Participants were a series of 13 Japanese patients including 11 males and two females, aged 38–92 yr, who had already been diagnosed with PAD and hospitalized in our department from June 2003 to August 2005 (Table 1). Patients classified as Fontaine's classes II–IV or with characteristic symptoms of PAD were included. Diseases accompanying PAD were defined as follows: type 2 diabetes mellitus, following the diagnostic criteria of Japan Diabetes Society; hypertension, blood pressure is equal to or greater than 140/90 mm Hg; end-stage renal disease, chronic renal failure on indispensable renal replacement therapy; ischemic heart disease, history of angina pectoris or myocardial ischemia with or without present medication; CHF, past diagnosis of CHF with or without present medication; hyperlipidemia, low-density lipoprotein-cholesterol is equal to or greater than 140 mg/dl, or triglyceride is equal to or greater than 150 mg/dl; obesity, body mass index is greater than 25 kg/m^2. Exclusion criteria were contraindications for carperitide: possibility of immediate surgery, suffering from malignancy, febrility, an inability to declare subjective symptoms, pregnancy, or other unfavorable statuses. The study was conducted in accordance with the guidelines in the Declaration of Helsinki. The study protocol was approved by the Ethics Committee Graduate School and Faculty of Medicine, Kyoto University. Patients were fully informed of the aim of the study, and their written informed consent was obtained.

Procedure of carperitide administration to patients

Carperitide was administered continuously and iv for 2 wk for Fontaine I–III patients and for 4 wk for Fontaine IV patients in principle. The starting dose of 0.006 μg/kg·min was gradually increased as long as the systolic blood pressure remained above 100 mm Hg. The range of final

TABLE 1. Patients' characteristics

Characteristic	n
Sex	
Male	11
Female	2
Diagnosis	
Arteriosclerosis obliterans	12
Thromboangitis obliterans	1
Gangrene or ulcer(s)	4
Fontaine's classification	
I	1
II	5
III	2
IV	5
Other disorders	
Hypertension	12
Type 2 diabetes	11
ESRD	7
CHF	5
Ischemic heart disease	4
Hyperlipidemia	4
Obesity (BMI > 25)	3

Patients' mean ± SD age was 72 ± 15 yr. BMI, Body mass index.

doses of carperitide used in this study was 0.003–0.1 μg/kg·min. Drugs for injection such as prostaglandins were avoided during the carperitide administration. The administration was stopped and standard remedy performed if any unfavorable symptoms appeared.

Pain was assessed when present with a numerical rating scale from 0–10; grade 0 indicated no pain and grade 10 the strongest pain the patient could imagine. The ankle-brachial pressure index (ABI) was assessed by an automated measurement device (BP-203RPEII; Colin Medical Technology Corp., Aichi, Japan). An exercise tolerance test was carried out weekly for patients with intermittent claudication. Pain-free walking distance on a flat ground was assessed. A stair-climb test was performed when walking on flat ground did not induce claudication. The test assessed how many floors a patient could climb without pain on the stair of our internal medicine ward building. Blood sampling was performed immediately before the beginning of carperitide administration and weekly during the administration for routine blood examination. It was also performed to determine the plasma levels of ANP, cGMP, and vascular endothelial growth factor (VEGF).

Analysis of blood samples

The blood samples from mice were withdrawn in an ice-cold tube containing 0.5 M Na-EDTA final concentration and mixed well. Aprotinin was added at 500 U/ml when a sample was used for human ANP measurement. The plasma was immediately isolated by a centrifugation and stored at −20 C until further processing. Plasma concentrations of cGMP, VEGF, and human ANP were analyzed by SRL, Inc. (Tokyo, Japan).

Statistical analysis

Results are presented as mean ± SEM unless otherwise indicated. The statistical significance of differences in means was evaluated by ANOVA supplemented with Fisher's least-significant difference in comparisons among three or more groups in animal experiments and by paired *t* tests between before and after the carperitide administration in the human study. A P value < 0.05 was considered significant.

Results

Animal experiments

Angiogenesis was impaired in diabetic mice

Blood glucose levels in STZ-diabetic mice, on which the hind-limb ischemia was induced at 4, 16, and 26 wk after STZ injections, were 354 ± 151 mg/dl (n = 9), 354 ± 38 mg/dl (n = 9), and 308 ± 23 mg/dl (n = 9), respectively, on the day of surgery. In control nondiabetic mice, blood glucose levels at 4 wk after the injection of vehicle were 139 ± 4 mg/dl (n = 6), 132 ± 2 mg/dl (n = 9), and 131 ± 4 mg/dl (n = 9) for mice operated at 4, 16, and 26 wk, respectively, after the vehicle injection.

At 4 wk after the induction of diabetes, blood flow recovery of the STZ-diabetic group was similar to that of nondiabetic controls (Fig. 1A). But after a long-term hyperglycemic state of 16 or 26 wk, recovery was suppressed in the STZ-diabetic group by 26 or 32%, respectively, when compared with the control mice (Fig. 1, B and C).

ANP administration restored angiogenesis in diabetic mice

To investigate whether ANP can improve the impairment of blood flow recovery, carperitide was administered to C57BL/6 mice in which femoral artery ligation was made after a 16-wk exposure to hyperglycemia.

Blood glucose levels at femoral artery ligation were 116 ± 4 mg/dl in the vehicle-treated nondiabetic group, 122 ± 3 mg/dl in the carperitide-treated nondiabetic group, 343 ± 42 mg/dl in the vehicle-treated STZ-diabetic group, and 366 ± 42 mg/dl in the carperitide-treated STZ-diabetic group. In nondiabetic mice, the carperitide administration significantly accelerated blood flow recovery compared with the vehicle-treated group. The ischemic/normal limb blood flow ratio measured at 21 d after the surgery was 0.58 ± 0.03 in the vehicle-treated nondiabetic group (n = 13) and was significantly augmented in the carperitide-treated nondiabetic group (0.74 ± 0.06, n = 7; $P < 0.05$). The accelerating effect of carperitide on blood flow recovery was also seen in STZ-diabetic mice. The ischemic/normal limb blood flow ratio at

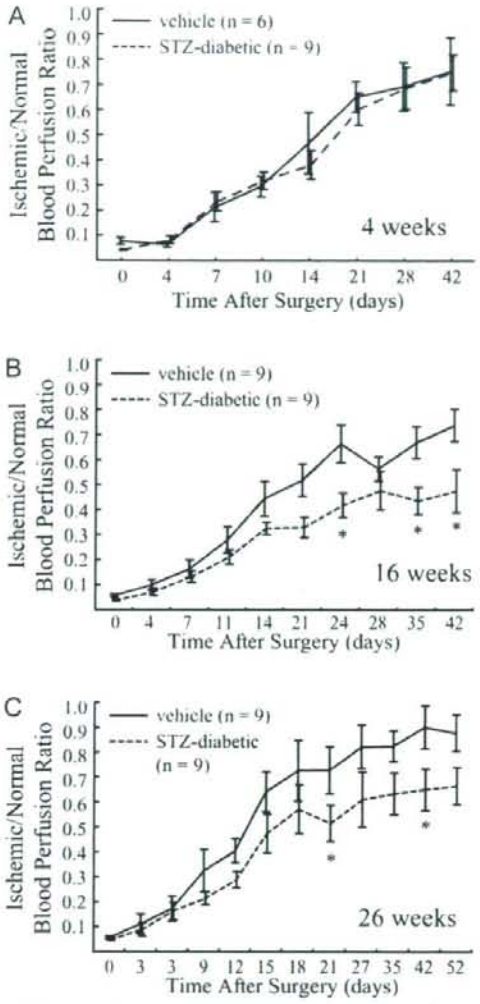

FIG. 1. Impairment of ischemia-induced blood flow recovery in mice with diabetes. Blood flow recovery after femoral artery ligation assessed by an ischemic/normal blood perfusion ratio was not altered 4 wk after STZ administration (A) but was significantly delayed 16 wk (B) and 26 wk (C) after induction of diabetes compared with vehicle-treated nondiabetic controls.*, $P < 0.05$ *vs.* vehicle-treated mice at each time point by ANOVA.